Determinants of workplace exposure and release of ultrafine particles during atmospheric plasma spraying in the ceramic industry

Viana M.[1], Fonseca A.S.[2], Querol X.[1], López-Lilao A.[3], Carpio P.[3,4], Salmatonidis A.[1], Monfort E.[3],

[1]Institute of Environmental Assessment and Water Research (IDÆA-CSIC), C/ Jordi Girona 18, 08034 Barcelona, Spain.
[2]National Research Centre for the Working Environment (NRCWE), Lersø Parkallé 105, 2100 Copenhagen, Denmark.
[3]Institute of Ceramic Technology (ITC)- AICE - Universitat Jaume I, Campus Universitario Riu Sec, Av. Vicent Sos Baynat s/n, 12006 Castellón, Spain.
[4]Institute of Materials Technology (ITM), Universtiat Politècnica de València, Camino de Vera s/n, 46022 Valencia, Spain.

Abstract

Atmospheric plasma spraying (APS) is a frequently used technique to produce enhanced-property coatings for different materials in the ceramic industry. This work aimed to characterise and quantify the impact of APS on workplace exposure to airborne particles, with a focus on ultrafine particles (UFPs, <100 nm) and nanoparticles (<50 nm). Particle number, mass concentrations, alveolar lung deposited surface area concentration, and size distributions, in the range 10 nm – 20 µm were simultaneously monitored at the emission source, in the worker breathing zone, and in outdoor air. Different input materials (known as feedstock) were tested: (a) micro-sized powders, and (b) suspensions containing submicron- or nano-sized particles. Results evidenced significant UFP emissions (up to $3.3x10^6/cm^3$) inside the projection chamber, which impacted exposure in the breathing zone outside the projection chamber (up to $8.3x10^5/cm^3$). Environmental release of UFPs was also detected and quantified ($3.9x10^5/cm^3$). Engineered nanoparticle (ENP) release to workplace air was also evidenced by TEM microscopy. UFP emissions were detected during the application of both micro-sized powder and suspensions containing submicron- or nano-sized particles, thus suggesting that emissions were process- (and not material-) dependent. An effective risk prevention protocol was implemented, which resulted in a reduction of worker UFP exposure in the breathing zone. These findings evidence the potential risk of occupational exposure to UFPs during atmospheric plasma spraying, and raise the need for further research on UFP formation mechanisms in high-energy industrial processes.

Keywords: process-generated particles, engineered nanoparticles, pristine nanoparticles, mitigation strategies, occupational health, indoor air quality, thermal plasma spraying.

1. Introduction

Thermal spraying in general, and atmospheric plasma spraying (APS) in particular, are frequently used technologies to produce high-performance surfaces required in industrial processes. APS is used to deposit different coatings on a number of surfaces in order to achieve enhanced properties such as wear, corrosion, electrical insulation or heat resistance, while maintaining the structural properties of the underlying material (Fauchais et al., 2014; Rosso et al., 2001; Stöver and Funke, 1999). Atmospheric plasma spraying is commonly employed because of its versatility and wide applicability in diverse technologies such as coating of stainless steel components (e.g., pistons) to prevent wear and corrosion in pump applications, coating of metal structures (e.g., turbine engines and blades) to obtain ceramic thermal barriers in aero-spatial and energy-generation applications, or rapid manufacturing of metal molds without limitation of pattern size, among others (Carpio et al., 2015a,b,c; Huang et al., 2016; Khor and Gu, 2000; Montanari et al., 2002; Olding et al., 2001; Tamulevičius and Dargis, 1998; Zhang et al., 2001).

During thermal spray deposition, the feedstock (starting material) is molten (or partially molten) and accelerated to impact onto the substrate surface, where the deposited material is cooled forming the coating. In the case of APS, the energetic source is a thermal plasma which achieves high impact velocities and very high temperatures (> 10000K). Plasma spraying can provide coatings with varying thickness over a large area at high deposition rate, which makes it advantageous with regard to other coating processes such as physical or chemical vapour deposition (Papyrin et al., 2007; Pawlowski, 1995). Another advantage is that the coated surface does not heat up significantly, allowing the coating of flammable substances. Furthermore, the high energy density and high temperature of plasma flow facilitate the deposition of coatings of refractory materials which are difficult to melt using other conventional thermal spraying techniques (Fauchais et al., 2014). Coating materials available for plasma spraying include metals, alloys, ceramics, plastics and composites, which are typically fed in micro-sized powder form. The use of nanoparticles (<50 nm, NPs) as a feedstock can improve the properties of the coatings (Pawlowski, 2009). However, nanoparticles cannot be injected directly inside the plasma plume because of their poor flowability and low specific weight. For this reason, the injection of suspensions (containing submicron- or nano-sized particles) instead of micro-sized powders has been implemented in recent years. This modification is named suspension plasma spraying (SPS) and the phenomena (fusion, evaporation, particle trajectory, etc.) which occur inside the plasma plume change significantly with respect to the APS technique. (Pawlowski, 2009).

High-energy industrial processes similar to plasma spraying are known to release NPs and ultrafine (<100 nm, UFP) particles into workplace air (Fonseca et al., 2015, 2016a). These particles are usually referred to as process-generated particles (Broekhuizen et al., 2012), and they have the potential to impact indoor air quality, workplace exposure and human health (Li et al., 2016). Studies have shown that one thermal spraying technique similar to plasma spraying, high velocity oxy-fuel (HVOF) spraying, may even generate emissions of large dust particles above 10 µm in size (Huang et al., 2016). In addition to process-generated particles, workplace exposure may be affected by the unintentional release of engineered NPs (ENPs). The use of nanomaterials in

state-of-the-art industrial processes such as APS has increased in recent years, and it is expected that this trend will continue in the near future (Savolainen et al., 2013). Consequently, it is critical to identify any potential risks they may pose to human health in indoor, workplace and outdoor environments in the vicinity of the industrial emission source. The evaluation and characterisation of exposure scenarios and risks to airborne UFPs (whether process-generated or engineered) is addressed by the emerging field of research of nanosafety (Savolainen et al., 2013). The need for effective risk governance, which is crucial when developing new technologies and industrial processes, has been evidenced (Read et al., 2016).

In this framework, the present work aimed to assess UFP emissions and their potential impact on workplace exposure during atmospheric plasma spraying of ceramic coatings in an industrial setting. UFP release to the environment was also assessed. Moreover, a prevention protocol was implemented and the exposure levels reduction was quantified. Because of the different terminologies used in the air quality and the nanotechnology research fields, for the purpose of this work the following terms will be used: ultrafine particles (<100 nm), and nanoparticles (<50 nm). Particle diameters measured in this work are mainly submicron, but given that approximately 80% of particle number concentrations (N) is generally <100 nm, the term UFP will be used as equivalent to N even if they are not exactly the same.

2. Experimental setup

Atmospheric plasma spraying was carried out in an industrial-scale pilot plant located in the facilities of the Institute of Ceramic Technology (ITC) in Castellón, Spain. The APS system consisted in a monocathode plasma torch (F4-MB, Oerlikon-Metco, Switzerland) operated by a six-axes robot arm (IRB 1400, ABB, Switzerland). Due to standard occupational health and safety considerations, plasma spraying in the pilot plant is performed inside a closed chamber, with no direct interaction by the worker (Figure S1 in Supporting Information). The projection chamber (3x3x2.5 m^3) was located inside the worker's room (approximate dimensions 6x6x3 m^3), where the breathing zone was located at approximately 1.5 m from the projection chamber.

A total of 14 APS processes were carried out, 9 of which using micro-sized powders and 5 using aqueous suspensions containing submicron- or nano-sized particles as feedstock (Table 1). The following particle monitoring instrumentation was deployed:

- In the worker's room, outside the projection chamber (Figure S1 and S2; Zone A): a DiscMini particle counter (Testo) monitoring particle number concentrations (N) between 10-700 nm and mean particle diameter (D_p) was deployed next to the worker's desk, at breathing height. Appropriate conductive tubing (Asbach et al., 2015; Viana et al., 2015) was used. A butanol condensation particle counter (CPC, TSI Model 3775), monitoring particles between 4 and 1500 nm, was also used. Particle mass concentrations were monitored by means of a Grimm 1107 laser spectrometer, measuring PM_{10}, $PM_{2.5}$ and PM_1 concentrations. Particle samples for TEM-EDX analysis were collected on Au grids using SKC cassettes attached to a Leland Legacy pump operating at 6 L/min.

- Inside the projection chamber (Figure S1 and S2; Zone B): N concentrations were monitored using a second DiscMini unit. Particle number size distributions between 10-420 nm were monitored by means of a portable SMPS NanoScan (Fonseca et al., 2016b; Stabile et al., 2014; Tritscher et al., 2013), which was placed for safety reasons outside of the projection chamber and connected with conductive tubing (Tygon conductive tubing, 1.5 m in length) to the inside of the chamber. The authors are aware that the length of the tubing may result in particle losses and is thus a limitation of the study. Samples for the characterisation of particle morphology and composition by TEM-EDX were collected using a 3-stage rotating impactor (1 - 2.5 µm, 2.5 - 10 µm, and > 10 µm) using Au grids as collection substrates.

- Outdoor air: a third DiscMini unit and a second Grimm 1107 unit were deployed outdoors on the building's roof and at approximately 1 m from the ventilation exhaust originating from the worker's room, to monitor N, D_p, PM_{10}, $PM_{2.5}$ and PM_1. The instruments were located as close as possible to the exhaust (taking into account the operational limitations) while avoiding interference from other exhaust systems. The inlets were not located inside the exhaust to avoid instrumental failures, since these instrument are not adapted to work in duct streams.

All DiscMini and Grimm 1107 units were intercompared prior to the experiments at the IDAEA-CSIC urban background air quality monitoring station in Barcelona, monitoring outdoor air. One DiscMini was identified as the internal reference, and the other units were corrected (with slope and intercept) with regard to it. Correlation coefficients (R^2) between the different units were always >0.8. The Grimm 1107 spectrometers were corrected individually by comparison with EU reference high-volume samplers for PM_{10} and $PM_{2.5}$ mass concentrations. The DiscMini particle counters were also compared with a TSI SMPS3080 system coupled with a CPC3772 and showed a R^2>0.88 correlation with regard to N and a 12-18% relative difference with regard to D_p (Viana et al., 2015). The particle number concentration data were not corrected with regard to the SMPS given the different lower cutoff sizes of the DiscMini units and SMPS system. Finally, the butanol CPC was intercompared with the DiscMini units on site during a non-activity period (night-time), obtaining a correlation of R^2=0.87. The CPC data were not corrected with regard to the DiscMini units due to their different cutoff sizes, as in the case of the SMPS. The different particle size ranges of the instruments (10-700 nm for DiscMini, 4 nm to 1.5 µm for CPC) should be taken into account when intercomparing the different types of instruments.

Different feedstock types were tested in order to assess their influence on UFP emissions (Table 1), including:

Powders:

- Feedstock P1: ceramic glass powders made up of Na_2O, SiO_2, CaO, and P_2O_5. Its size distribution was micro-sized (<63 µm) with 1% of fluidized SiO_2 NPs (Cañas et al., 2016).
- Feedstock P2: commercial micro-scaled powder of a Ni-based superalloy (AMDRY 997, Oerlikon-Metco, Switzerland) with a mean particle size of 40 µm.

Suspensions:

- Feedstock S1: aqueous suspension containing a mix of lab-synthetized nano-sized particles of $Gd_2Zr_2O_7$ (60nm) and submicron-sized particles of ZrO_2-Y_2O_3 (Tosoh TZ-3YS, 400nm).
- Feedstock S2: aqueous suspension containing nano-sized particles ($Gd_2Zr_2O_7$).
- Feedstock S3: aqueous suspension containing submicron-sized particles (ZrO_2-Y_2O_3).

In order to reduce the exposure levels after they were detected (section 3), mitigation strategies were implemented according to a hierarchical prevention protocol:

- Stage 0: The APS system worked as it was set up by the manufacturer. Plasma spraying took place inside a cabin (projection chamber) with an air ventilation system where the air entrance was by a single point from the breathing zone.
- Stage 1: Corrective measures were applied in the emission zone (APS projection chamber; Figure S1 and S2 at Zone B).
- Stage 2: Corrective measures were applied to the air extraction system.
- Stage 3: Corrective measures were applied in the breathing zone (Figure S1 and S2; Zone A).

Detailed information of the applied corrective measures is provided in section 3.2. A summary of the APS experiments carried out may be found in Table 1, showing the feedstocks used, the number of replicas available, and the specific characteristics of the experimental setup.

3. Results and discussion

3.1. UFP emissions during plasma spraying

Particle number concentrations and size distribution were monitored inside the plasma chamber during the application of different feedstock as coatings. Background UFP number concentrations were representative of typical concentrations in an urban area (1.6×10^4/cm^3; Pérez et al., 2010; Reche et al., 2011), with D_p ranging between 40-70 nm characteristic of aged diesel exhaust aerosols (Brines et al., 2016; Dall'Osto et al., 2012). The influence of outdoor aerosols was high given that the doors of the pilot plant were open and connected directly to outdoor air.

Inside the chamber, results evidenced intense UFP emissions (Figure 1) coinciding with the spraying events. Particle number concentrations increased by up to 3 orders of magnitude inside the chamber (in the order of 10^6/cm^3) with respect to background concentrations (10^3-10^4/cm^3, Table 2) inside the chamber prior to spraying. This pattern was consistent across the different replicas (Figure 1). In the example shown in Figure 1, as the spraying process was initiated (after closing the chamber doors) UFP concentrations increased coinciding with the ignition of the plasma plume. During this stage, average 10-second UFP concentrations reached 2.1×10^4/cm^3 in the projection chamber, to subsequently peak at 6×10^6/cm^3 with a Dp of 25-30 nm during spraying of the feedstock. The emission pattern and measured UFP concentrations and Dp were mostly consistent across replicas. UFP formation may occur during three stages of thermal spray: (a) heating and melting of the feedstock, (b) acceleration of the droplets, and (c) impact and deposition stage. During these stages, UFPs are likely to be formed through vaporisation and subsequent nucleation of emission gases, or through

mechanical impaction (Huang et al., 2016). They may also be formed by nucleation linked to the emission of sulphur-containing gaseous precursors if these are present in the feedstock (Fonseca et al., 2016a). As shown in Figure 1, the data monitored by the two particle counters deployed inside the chamber (DiscMini and NanoScan) were also consistent, thus confirming the high absolute concentration values measured despite the fact that the peak concentrations were outside the concentration range recommended by the instrument manufacturers (>10^6/cm^3).

The results from this study evidence the formation and release of UFPs during plasma spraying. A previous study focusing on a different kind of high velocity spraying (HVOF) reported coarse particle emissions (>10 µm in size) with a unique morphology of polygonal or irregular block of crushed powder, and finer dust particles (2.5 µm) in the form of irregular or flocculent agglomerates (Huang et al., 2016). The authors monitored particle mass concentrations (PM, as opposed to N in this work) reaching maximum concentrations of 140 mg/m^3, with time-weighted average concentrations of 34 mg/m^3. In such a highly polluted scenario PM concentration should be the preferred exposure metric. Due to the particle concentration levels monitored in the scenario assessed in the present work, N was considered a more targeted metric for emissions and exposure monitoring (Vogel et al., 2014). To the authors' knowledge, Huang et al. (2016) is the only previous publication available monitoring particle release and exposure due to plasma spraying.

The experimental setup described above was replicated for the different kinds of feedstock shown in Table 1, with the results shown in Figure 2 and Table 2. Plasma spraying generated high UFP emission concentrations under all scenarios, which ranged between 2.6×10^6 and 3.3×10^6/cm^3 for experiments #1 to #3, and between 1.1×10^6 and 2.5×10^6/cm^3 for experiments #4 to #7. This relative decrease was probably linked to the implementation of mitigation strategies which will be discussed below. The mean Dp distribution monitored during experiments carried out at different stages of the prevention protocol is shown in Figure S3 in Supporting Information, including the following experiments: #2 and #3 (stage 1), #4 (stage 2) and #7 (stage 3). Aside from the differences obtained owing to the mitigation strategies, results evidence that major UFP emissions were generated during the application of both nano- and micro-sized suspensions and powders, thus suggesting that the emissions are related to the process and not only to the grain size distribution of the input material. This is consistent with previous results (Huang et al., 2016). The feedstocks applied during experiments #4, #6 and #7 were characterised by mean D_p of 60 and 400 nm ($Gd_2Zr_2O_7$, and ZrO_2-Y_2O_3, respectively), whereas the remaining materials were predominantly micro-sized (<63 µm) with only minor contributions (1%) from nanomaterials in the case of ceramic glass powders. As shown in Figure 2, mean D_p inside the chamber did not vary significantly across experiments and ranged between 28 nm in experiment #2 (micro-scaled feedstock) and 45 nm in experiment #6 (nano-scaled feedstock), and showed no consistent pattern for either type of material. As a result, it may be concluded that UFP emissions from APS are process-related. No statistically relevant conclusions can be drawn with regard to N emitted with the different types of coatings due to the fact that the measurements were carried out under different exhaust ventilation conditions inside the chamber.

In order to characterise their morphology and chemical composition inside the chamber particles were sampled on TEM grids. It should be noted that TED-EDX results are not quantitative, and refer to single particles identified. As expected, different particle morphologies were observed. Figure 3a shows an example of spherical particles originating from evaporation and condensation or fusion of the feedstock, in this case originating from the aqueous suspension containing submicron-sized particles (ZrO_2-Y_2O_3). In addition, release of the pristine (original) ENPs was also identified (Figure 3b), in the case of the Gd-based ENPs. Mauer et al. (2015) reported the difficulties in coating with $Gd_2Zr_2O_7$ due to the fact that the material is partly decomposed inside the plasma plume and the Gd_2O_3 is evaporated. Thus, this confirms that the ENPs detected by TEM may have been originated due to a partial evaporation of the feedstock and subsequent condensation of the vapour. Given the high correlation between particle concentrations in the plasma chamber and in the worker breathing zone (Figure 4), it is expectable that exposures to the ENPs detected inside the chamber occur in the breathing zone. Further studies are necessary to confirm this hypothesis. Finally, Ca-rich particles probably sourcing from the feedstock (Figure 3c) were also observed. These results are also consistent with the variety of particle morphologies detected in previous studies (Huang et al., 2016).

3.2. *Impact on exposure*

Worker exposure to UFP emissions from the plasma chamber was assessed by placing monitoring instruments on a desk in close proximity to the worker and at breathing height, thus closely simulating breathing zone conditions (Asbach, 2015; Vogel et al., 2014). Plasma spraying activities inside the chamber had an evident and statistically significant impact (>background + $3.\sigma_{background}$; Asbach et al. 2012) in the breathing zone (Figure 4). Breathing zone UFP concentrations followed an increasing pattern coinciding with the start of the spraying process, but with a 1-2 minute delay due to transport from the chamber towards the breathing zone. In the example shown in Figure 4*,* representative of experiments #2 to #3 (stage 1), UFP concentrations increased from $2.2\times10^4/cm^3$ prior to the spraying activity to $7.2\times10^5/cm^3$ during and after spraying. Mean D_p increased by 10-20 nm (Table 2) with regard to those measured inside the plasma chamber probably due to particle transport and ageing between the two measurement locations (approximately 2 m). The uncertainty of the monitoring instrumentation should evidently be taken into account for this assessment. As a result it may be concluded that, for experiments #1 to #3, the exhaust system in place was able to remove between 68% and 91% of the UFP monitored inside the plasma chamber, resulting in significant exposure concentrations in the breathing zone and with potentially health hazardous D_p (33-51 nm; Table 2).

Aside from the actual spraying periods, worker exposures also occurred during cleaning (by using a vacuum cleaner) of the chamber at the end of each spraying process. As expected, this activity impacted PM_{10} and $PM_{2.5}$ concentrations due to the coarser D_p of the particles re-suspended, with concentrations increasing from 5 to 350 $\mu gPM_{2.5}/m^3$ (Figure 5). Conversely, emissions from direct APS had only minor impacts on $PM_{2.5}$ mass. Even though these results may seem to contrast with previous studies (Huang et al., 2016), it is probable that the cause are the different concentration and exposure ranges in both plasma spraying scenarios, possibly influenced by the different technologies applied (APS *vs*. HVOF).

In order to reduce exposure concentrations, the prevention protocol described in the Methods section was applied by implementing the following measures:

- Stage 1: Improved air circulation in the plasma chamber using a multi-point system surrounding the plasma flame, as well as a delayed door-opening protocol. The air intake into the plasma room was changed from the breathing zone to directly from outdoor air.
- Stage 2: Enhanced sealing of the extraction system ducts from the chamber to the exhaust, to prevent the flow of emissions towards the breathing zone.
- Stage 3: Enhanced air exchange rates through forced ventilation in the breathing zone (to approximately 14 air exchanges per hour, in contrast to the original 2 air exchanges per hour).

Reductions in exposure concentrations in the breathing zone are evident after the implementation of the mitigation strategies (Figure 2). The comparison between experiments #1 and #2 evidences a reduction of UFP concentrations of approximately 70% (from 8.3×10^5 to 2.7×10^5/cm^3, monitored with DiscMini). Likewise, the comparison between experiments #3 and #6 shows a 75% reduction of UFP concentrations between stages 1 and 3 (from 1.8×10^5 to 4.4×10^4/cm^3, monitored with the CPC). Even though the reductions observed are experiment-dependent and data are not available from the same instrument for all experiments for direct comparison, these results evidence the benefits of the exposure mitigation protocol implemented. Exposure reductions were monitored in the breathing zone, while concentrations remained relatively constant (same order of magnitude) inside the projection chamber.

Finally, UFP concentrations in the breathing zone after the implementation of the mitigation strategies (1.9×10^4/cm^3, measured with the CPC) were comparable to those monitored in urban environments in European cities as such as Barcelona, London or Bern (1.2×10^4-2.8×10^4/cm^3; Reche et al., 2011). However, it should be taken into account that the exposure risk also depends on the coating chemical composition which in some cases may include potentially health hazardous materials.

3.3. Impact on environmental release

In addition to exposure, APS emissions impacted outdoor air. Environmental release of UFPs, monitored on the rooftop of the pilot plant (5 m above ground) in the vicinity of the exhaust system (1 m), was evidenced through a 1-order of magnitude increase in UFP concentrations (1.7×10^4/cm^3 to 2.5×10^5/cm^3; Figure 4), which was again observed across all replicas (Figure 1). As in the case of the breathing zone, this increase should also be considered statistically significant (Asbach et al., 2012). However, no environmental or health impacts should be expected from this specific pilot plant due to (a) the short temporal impact of the emissions (<2 min), (b) their fast dilution in outdoor air, (c) the fast coagulation/agglomeration of particles and thus their increase in particle diameter, and (d) the chemical composition of the feedstock used in these experiments, resembling mineral matter. Despite this, APS may be used to apply a broad variety of coatings which include potentially health hazardous metals (e.g., Cr, Co, W, etc.), in which case environmental release of such metal-rich UFPs should be monitored and prevented (Li et al., 2016) using appropriate gas cleaning systems.

4. Conclusions

Ultrafine particle emissions and their impact on workplace exposure were monitored during atmospheric plasma spraying (APS) in an industrial-scale pilot plant. Particle diameters monitored ranged between 10-700 nm but are reported as UFP given that 80% of total N is generally found in the <100 nm size range. UFP emissions were expected due to the high-energy nature of this industrial process. Results evidenced major UFP emissions during APS reaching up to $3.3\times10^6/cm^3$ inside the projection chamber with D_p ranging between 28-45 nm. Breathing zone concentrations reached up to $8.3\times10^5/cm^3$ (33-51 nm in diameter). These concentrations were statistically significantly higher than the initial background concentrations of 10^3-$10^4/cm^3$, and thus evidence the health hazardous potential of this industrial process. The nature of the emissions was investigated by testing micro- and nano-sized feedstocks, including engineered nanoparticles (ENPs). The mean D_p inside the APS chamber did not vary significantly across experiments and showed no consistent differences between the different feedstocks. Thus, it was concluded that UFP emissions were detected irrespective of the presence of ENPs in the feedstock, and that they were therefore process-related. In a minor proportion, release of pristine ENPs to the plasma chamber air was also evidenced by TEM microscopy. New particle formation originating from the evaporation of the feedstock was also detected. A risk prevention protocol was applied to the studied facility, leading to significant reductions in breathing zone UFP concentrations. This work evidences the relevance of process-generated emissions with regard to workplace exposure to nanoparticles, and the need for real-world assessments in order to identify exposure risks and improve indoor air quality in industrial settings by implementing effective prevention protocols.

5. Acknowledgements

This project was supported by the Spanish MINECO through project PCIN-2015-173-C02-01, under the frame of SIINN, the ERA-NET for a Safe Implementation of Innovative Nanoscience and Nanotechnology, by SIINN-ERANET project CERASAFE (id.:16). Support is also acknowledged to FP7 Marie Curie ITN HEXACOMM (Nr. 315760), Generalitat de Catalunya 2014 SGR33, the Department of Environmental Quality of the Generalitat de Catalunya, and the Spanish Ministry of the Environment (13CAES006).

References

Asbach, C., Kuhlbusch, T., Kaminski, H., Stahlmecke, B., Plitzko, S., Götz, U., Voetz, M., Kiesling, H.J., Dahmann, D. (2012). NanoGEM Standard Operation Procedures for assessing exposure to nanomaterials, following a tiered approach.

Asbach, C., 2015. Chapter 3.3 – Exposure Measurement at Workplaces, in: Nanoengineering. pp. 523–555. doi:10.1016/B978-0-444-62747-6.00016-6

Asbach, C., Kaminski, H., Beckmann, S., Monz, C., Dahmann, D., Fierz, M., Clavaguera, S., Faure, B., Dziurowitz, N., Meyer-Plath, A., Simonow, B., Iavicoli, I., Fontana, L., Fonseca, A.S., Viana, M., Todea, A.M., 2015. Field Applicability of Personal Monitors for Assessing Worker Exposure to Airborne Nanomaterials, in: European Aerosol Conference 2015, Milan, Italy.

Brines, M., Dall'Osto, M., Amato, F., Cruz Minguillón, M., Karanasiou, A., Alastuey, A., Querol, X., 2016. Vertical and horizontal variability of PM_{10} source contributions in Barcelona during SAPUSS. Atmos. Chem. Phys. 16, 6785–6804.

430 doi:10.5194/acp-16-6785-2016
431 Broekhuizen, P., Broekhuizen, F., Cornelissen, R., Reijnders, L., 2012. Workplace
432 exposure to nanoparticles and the application of provisional nanoreference values
433 in times of uncertain risks. J. Nanoparticle Res. 14, 1–25. doi:10.1007/s11051-
434 012-0770-3
435 Carpio, P., Borrell, A., Salvador, M.D., Gómez, A., Martínez, E., Sánchez, E., 2015a.
436 Microstructure and mechanical properties of plasma spraying coatings from YSZ
437 feedstocks comprising nano- and submicron-sized particles. Ceramics
438 International 41, Issue 3, Part A, 4108-41170. doi:10.1016/j.ceramint.2014.11.106.
439 Carpio, P., Bannier, E., Salvador, M.D., Borrell, A., Moreno, R., Sánchez, E., 2015b.
440 Effect of particle size distribution of suspension feedstock on the microstructure
441 and mechanical properties of suspension plasma spraying YSZ coatings. Surface
442 and Coatings Technology 268, 293-297. doi: 10.1016/j.surfcoat.2014.08.063.
443 Carpio, P., Moreno, R., Gómez, A., Salvador, M.D., Sánchez, E., 2015c. Role of
444 suspension preparation in the spray drying process to obtain
445 nano/submicrostructured YSZ powders for atmospheric plasma spraying. Journal
446 of the European Ceramic Society 35, Issue 1, 237-247. doi:
447 10.1016/j.jeurceramsoc.2014.08.008.
448 Dall'Osto, M., Beddows, D.C.S., Pey, J., Rodriguez, S., Alastuey, A., Harrison, R.M.,
449 Querol, X., 2012. Urban aerosol size distributions over the Mediterranean city of
450 Barcelona, NE Spain. Atmos. Chem. Phys. 12, 10693–10707. doi:10.5194/acp-12-
451 10693-2012
452 Fauchais, P.L., Heberlein, J.V.R., Boulos, M., 2014. Thermal Spray Fundamentals.
453 Springer.
454 Fonseca, A.S., Maragkidou, A., Viana, M., Querol, X., Hämeri, K., de Francisco, I.,
455 Estepa, C., Borrell, C., Lennikov, V., de la Fuente, G.F., 2016a. Process-
456 generated nanoparticles from ceramic tile sintering: Emissions, exposure and
457 environmental release. Sci. Total Environ. 565, 922–932.
458 doi:10.1016/j.scitotenv.2016.01.106
459 Fonseca, A.S., Viana, M., Pérez, N., Alastuey, A., Querol, X., Kaminski, H., Todea,
460 A.M., Monz, C., Asbach, C., 2016b. Intercomparison of a portable and two
461 stationary mobility particle sizers for nanoscale aerosol measurements. Aerosol
462 Sci. Technol. 50, 653–668.
463 Fonseca, A.S., Viana, M., Querol, X., Moreno, N., de Francisco, I., Estepa, C., de la
464 Fuente, G.F., 2015. Ultrafine and nanoparticle formation and emission
465 mechanisms during laser processing of ceramic materials. J. Aerosol Sci. 88, 48–
466 57. doi:10.1016/j.jaerosci.2015.05.013
467 Huang, H., Li, H., Li, X., 2016. Physicochemical Characteristics of Dust Particles in
468 HVOF Spraying and Occupational Hazards : Case Study in a Chinese Company.
469 J. Therm. Spray Technol. 25, 971–981. doi:10.1007/s11666-016-0422-8
470 Khor, K.., Gu, Y.., 2000. Thermal properties of plasma-sprayed functionally graded
471 thermal barrier coatings. Thin Solid Films 372, 104–113. doi:10.1016/S0040-
472 6090(00)01024-5
473 Li, N., Georas, S., Alexis, N., Fritz, P., Xia, T., Williams, M.A., Horner, E., Nel, A., 2016.
474 A work group report on ultrafine particles (American Academy of Allergy, Asthma
475 & Immunology): Why ambient ultrafine and engineered nanoparticles should
476 receive special attention for possible adverse health outcomes in human subjects.
477 J. Allergy Clin. Immunol. doi:10.1016/j.jaci.2016.02.023
478 Montanari, R., Riccardi, B., Volterri, R., Bertamini, L., 2002. Characterisation of plasma
479 sprayed W coatings on a CuCrZr alloy for nuclear fusion reactor applications.
480 Mater. Lett. 52, 100–105. doi:10.1016/S0167-577X(01)00375-5
481 Olding, T., Sayer, M., Barrow, D., 2001. Ceramic sol–gel composite coatings for
482 electrical insulation. Thin Solid Films 398–399, 581–586. doi:10.1016/S0040-
483 6090(01)01322-0
484 Papyrin, A., Kosarev, V., Klinkov, S., Alkhimov, A., V., F., 2007. Cold Spray

485 Technology. Elsevier, Oxford.
486 Pawlowski, L., 1995. The Science and Technology of Thermal Spray Coatings. Wiley,
487 New York.
488 Pérez, N., Pey, J., Cusack, M., Reche, C., Querol, X., Alastuey, A., Viana, M., 2010.
489 Variability of Particle Number, Black Carbon, and PM10, PM2.5, and PM1 Levels
490 and Speciation: Influence of Road Traffic Emissions on Urban Air Quality. Aerosol
491 Sci. Technol. 44, 487–499. doi:10.1080/02786821003758286
492 Read, S.A.K., Kass, G.S., Sutcliffe, H.R., Hankin, S.M., 2016. Foresight Study on the
493 Risk Governance of New Technologies: The Case of Nanotechnology. Risk Anal.
494 36, 1006–1024. doi:10.1111/risa.12470
495 Reche, C., Querol, X., Alastuey, A., Viana, M., Pey, J., Moreno, T., Rodríguez, S.,
496 González, Y., Fernández-Camacho, R., Campa, A.M.S. de la, Rosa, J. de la,
497 Dall'Osto, M., Prévôt, A.S.H., Hueglin, C., Harrison, R.M., Quincey, P., 2011. New
498 considerations for PM, Black Carbon and particle number concentration for air
499 quality monitoring across different European cities. Atmos. Chem. Phys. 11,
500 6207–6227.
501 Rosso, M., Scrivani, A., Ugues, D., Bertini, S., 2001. Corrosion resistance and
502 properties of pump pistons coated with hard materials. Int. J. Refract. Met. Hard
503 Mater. 19, 45–52. doi:10.1016/S0263-4368(00)00053-6
504 Savolainen, K., Backman, U., Brouwer, D., Fadeel, B., Fernandes, T., Kuhlbusch, T.,
505 Landsiedel, R., Lynch, I., Pylkkänen, L., 2013. Towards Safe and Sustainable
506 Nanomaterials and Nanotechnology Innovations. Työterveyslaitos.
507 Stabile, L., Cauda, E., Marini, S., Buonanno, G., 2014. Metrological assessment of a
508 portable analyzer for monitoring the particle size distribution of ultrafine particles.
509 Ann. Occup. Hyg. 58, 860–876.
510 Stöver, D., Funke, C., 1999. Directions of the development of thermal barrier coatings
511 in energy applications. J. Mater. Process. Technol. 92–93, 195–202.
512 doi:10.1016/S0924-0136(99)00244-7
513 Tamulevičius, S., Dargis, R., 1998. Application of plasma spray deposited coatings for
514 seawater activated batteries. J. Power Sources 72, 9–13. doi:10.1016/S0378-
515 7753(97)02808-5
516 Tritscher, T., Beeston, M., Zerrath, A.F., Elzey, S., Krinke, T.J., Filimundi, E., Bischof,
517 O.F., 2013. NanoScan SMPS – A Novel, Portable Nanoparticle Sizing and
518 Counting Instrument. J. Phys. Conf. Ser. 429, 12061.
519 Viana, M., Rivas, I., Reche, C., Fonseca, A.S., Pérez, N., Querol, X., Alastuey, A.,
520 Álvarez-Pedrerol, M., Sunyer, J., 2015. Field comparison of portable and
521 stationary instruments for outdoor urban air exposure assessments. Atmos.
522 Environ. 123, 220–228. doi:10.1016/j.atmosenv.2015.10.076
523 Vogel, U., Savolainen, K., Wu, Q., van Tongeren, M., Brouwer, D., Berges, M.,
524 Brouwer, D.H., Lidén, G., Asbach, C., Berges, M.G.M., van Tongeren, M., 2014.
525 Chapter 5 – Monitoring and Sampling Strategy for (Manufactured) Nano Objects,
526 Agglomerates and Aggregates (NOAA): Potential Added Value of the
527 NANODEVICE Project, in: Handbook of Nanosafety. pp. 173–206.
528 doi:10.1016/B978-0-12-416604-2.00005-6
529 Zhang, H., Wang, G., Luo, Y., Nakaga, T., 2001. Rapid hard tooling by plasma
530 spraying for injection molding and sheet metal forming. Thin Solid Films 390, 7–
531 12. doi:10.1016/S0040-6090(01)00910-5
532
533

Figure captions

Figure 1. Top: Particle number concentrations (N, 10-700 nm with DiscMini; 10-420 nm with NanoScan SMPS) monitored during 3 replicas in experiment #2, using a micrometric powder (Na_2O; SiO_2; CaO; P_2O_5; 1% nano) as feedstock, in the plasma chamber and in outdoor air. Bottom: Particle size distribution monitored during 3 replicas in experiment #2. The plasma spraying activity of each replica is shown as a horizontal line between grey circles.

Figure 2. Mean particle number concentrations (N) and particle diameter (D_p) inside the plasma chamber for each of the experiments performed.

Figure 3. TEM images of particles collected on TEM grids inside the plasma chamber. (a) spherical particles originating from evaporation of the feedstock (ZrO_2-Y_2O_3 nanoparticles), experiment #7; (b) release of pristine Gd-based ENPs, experiment #6; (c) mineral (Ca) particles probably sourcing from the feedstock, experiment #2.

Figure 4. Particle number concentrations (N, 10-700 nm with DiscMini; 4 nm to 1.5 µm with CPC) monitored during one of the replicas in experiment #2, using a micro-sized powder (Na_2O; SiO_2; CaO; P_2O_5; 1% nano) as feedstock. Measurements carried out in the plasma chamber, in the breathing zone, and in outdoor air. The plasma spraying activity is shown as a horizontal line between grey circles.

Figure 5. Impact of cleaning activities on particle mass concentrations ($PM_{2.5}$) in the plasma chamber. Work activities such as plasma spraying or cleaning are shown as a horizontal line between grey circles.

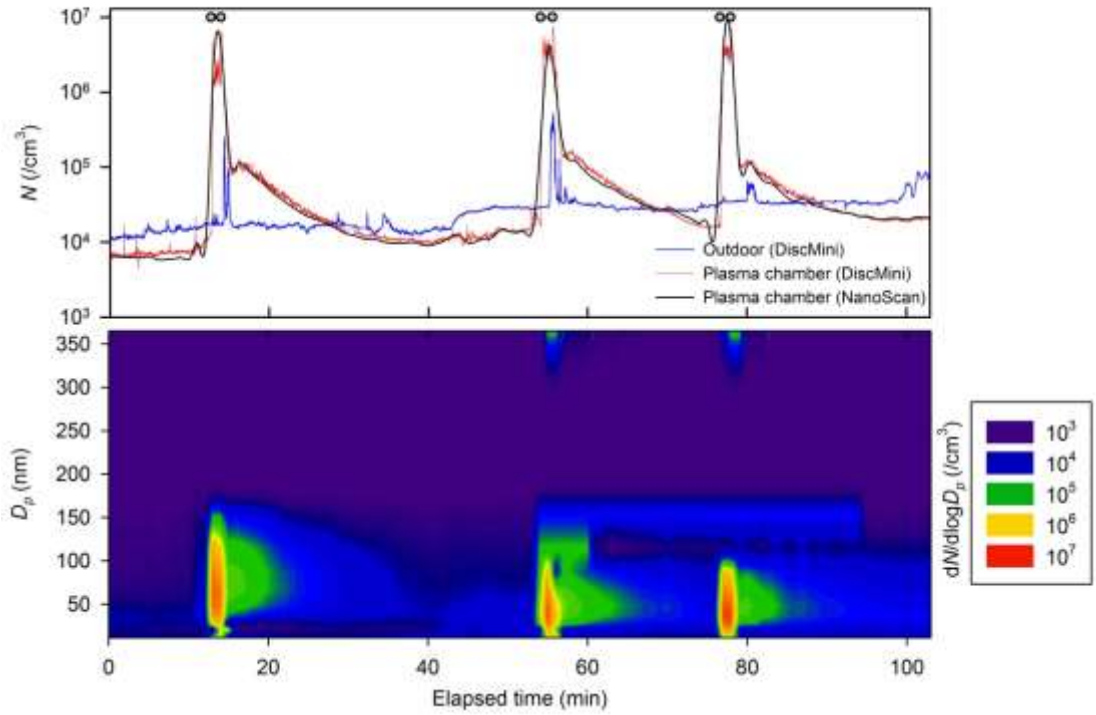

560

561 Figure 1

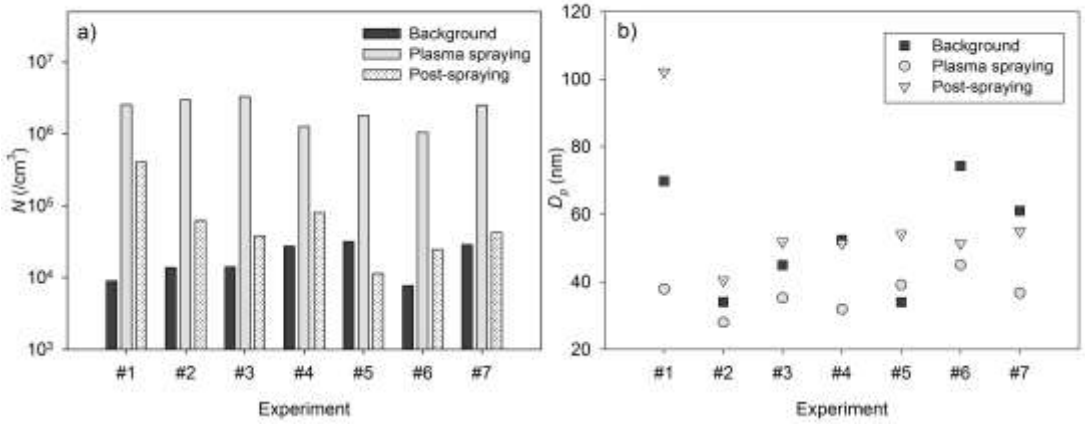

562
563

564 Figure **2**

565

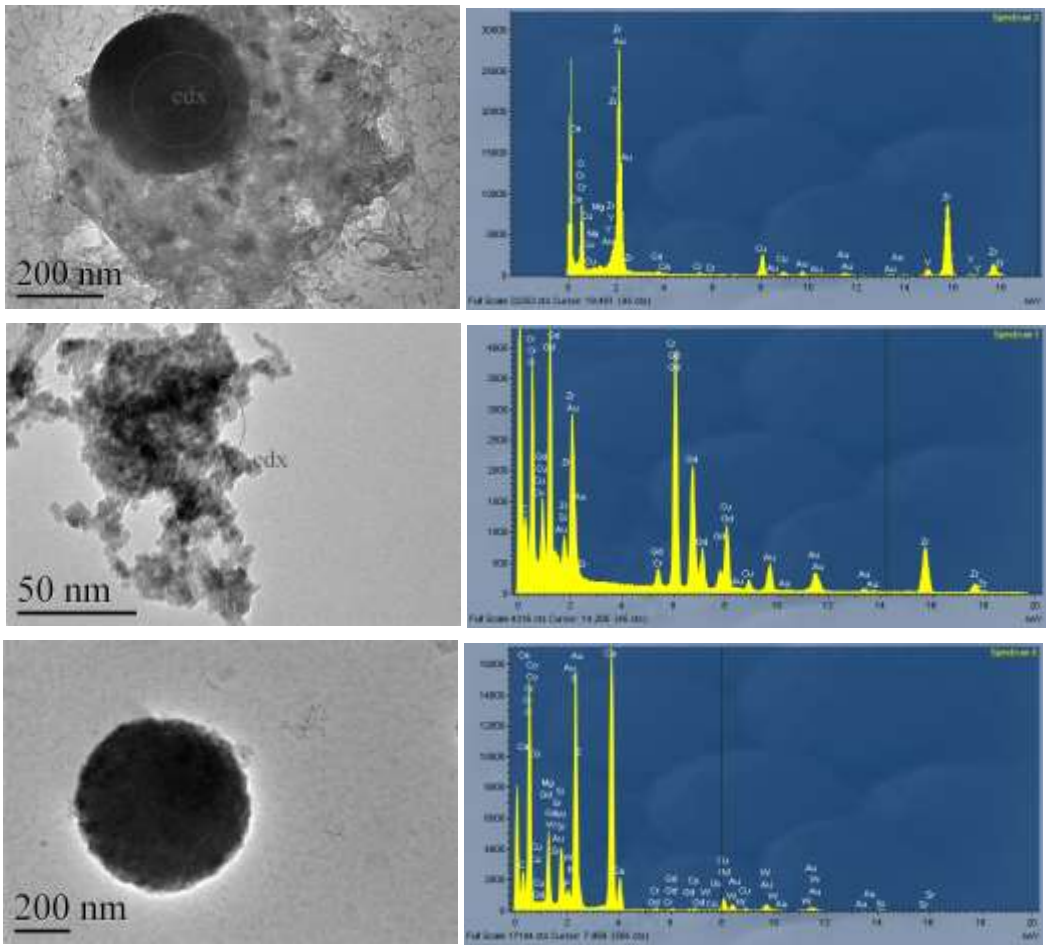

a) b) c)

Figure 3

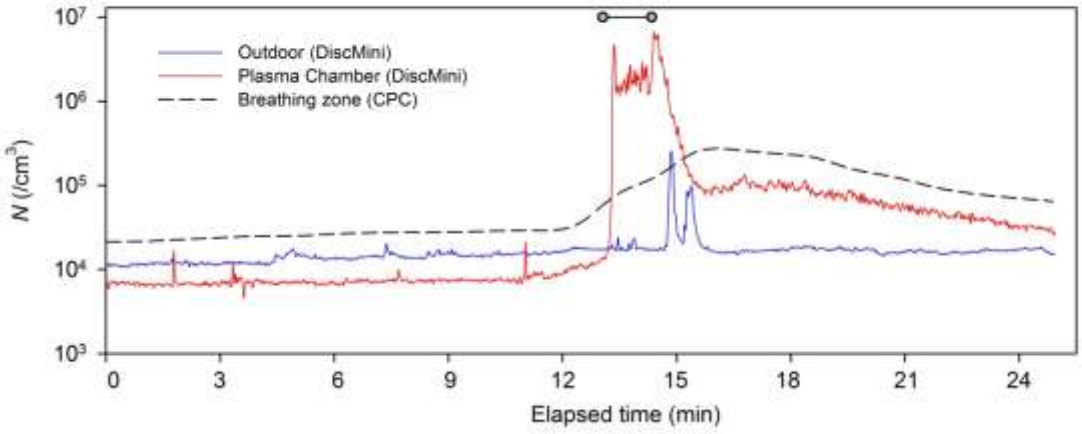

Figure 4

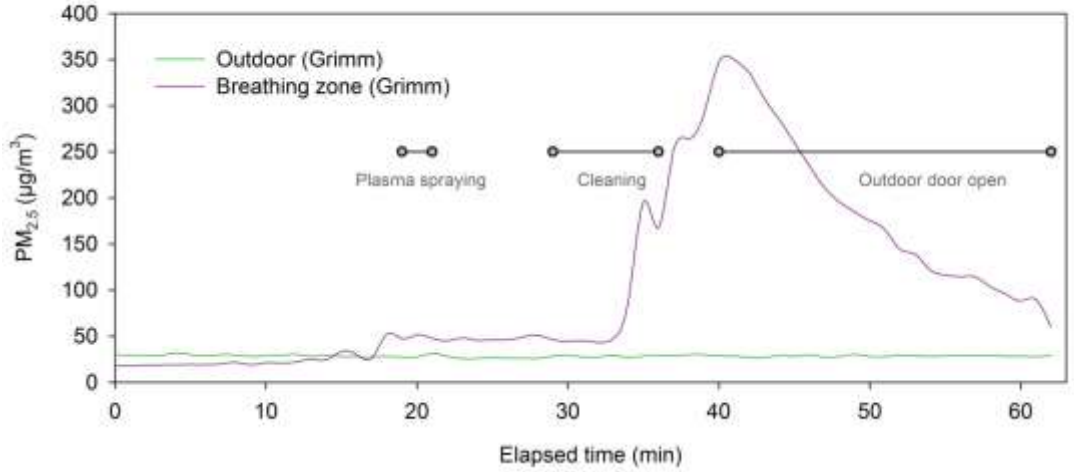

Figure 5

Table 1. Summary of plasma spraying experiments. Experimental setup: pre- or post-mitigation strategies. P: powder. S: suspension

Experiment (date)	Feedstock	Grain size (feedstock)	Composition	Replicas	Setup
#1 (31/10/15)	P1	Micro	Na_2O; SiO_2; CaO; P_2O_5 (1% nano)	1	Stage 0
#2 (17/12/16)	P1	Micro	Na_2O; SiO_2; CaO; P_2O_5 (1% nano)	4	Stage 1
#3 (17/12/16)	P2	Micro	NiCoCrAlTaY	1	
#4 (17/12/16)	S1	Submicro + Nano	ZrO_2-Y_2O_3 + $Gd_2Zr_2O_7$	1	Stage 2
#5 (08/01/16)	P2	Micro	NiCoCrAlTaY	3	Stage 3
#6 (08/01/16)	S2	Submicro	$Gd_2Zr_2O_7$	2	
#7 (08/01/16)	S3	Nano	ZrO_2-Y_2O_3	2	

588 Table 2. Mean UFP number concentrations and particle diameter inside the plasma chamber and in the breathing zone for each of the experiments
589 performed, prior to and during the spraying activity. Data not available in the breathing zone for experiments #5 to #7 due to instrumental failures.

590

Experiment	Feedstock Grain size	Setup	UFP (#/cm^3)							
			Plasma chamber				Breathing zone			
			Background		Plasma spraying		Background		Plasma spraying	
			DiscMini	NanoScan	Discmini	NanoScan	DiscMini	CPC	DiscMini	CPC
#1	Micro	Stage 0	9.0×10^3	9.5×10^3	2.6×10^6	7.9×10^5	9.8×10^3	N/A	8.3×10^5	N/A
#2	Micro	Stage 1	1.4×10^4	1.6×10^4	3.0×10^6	2.6×10^6	2.2×10^4	3.3×10^4	2.7×10^5	2.6×10^5
#3	Micro		1.4×10^4	2.0×10^4	3.3×10^6	3.2×10^6	2.8×10^4	2.6×10^4	7.2×10^5	1.8×10^5
#4	Submicro + Nano	Stage 2	2.7×10^4	2.9×10^4	1.3×10^6	1.7×10^6	2.6×10^4	3.2×10^4	2.9×10^5	5.2×10^4
#5	Micro	Stage 3	3.2×10^4	N/A	1.8×10^6	N/A	N/A	1.8×10^4	N/A	4.4×10^4
#6	Submicro		7.8×10^3	N/A	1.1×10^6	N/A	N/A	9.7×10^3	N/A	1.9×10^4
#7	Nano		2.9×10^4	2.7×10^4	2.5×10^6	1.3×10^6	N/A	N/A	N/A	N/A
			Size (nm)							
			Plasma chamber				Breathing zone			
			Background		Plasma spraying		Background		Plasma spraying	
			DiscMini	NanoScan	N Discmini	NanoScan	DiscMini	CPC	DiscMini	CPC
#1	Micro	Stage 0	70	64	38	59	61	-	47	-
#2	Micro	Stage 1	34	42	28	47	33		33	
#3	Micro		45	56	35	53	44		45	
#4	Submicro + Nano	Stage 2	52	62	32	48	52		51	
#5	Micro	Stage 3	34	N/A	39	N/A	N/A		N/A	
#6	Submicro		74	N/A	45	N/A	N/A		N/A	
#7	Nano		61	72	37	47	N/A		N/A	

591 N/A: not available

Supporting Information

Determinants of workplace exposure and release of ultrafine particles during atmospheric plasma spraying in the ceramic industry

Viana M.[1], Fonseca A.S.[2], Querol X.[1], López-Lilao A.[3], Carpio P.[3, 4], Salmatonidis A.[1], Monfort E.[3],

Figure S1. Projection chamber (left) and worker's room (right)

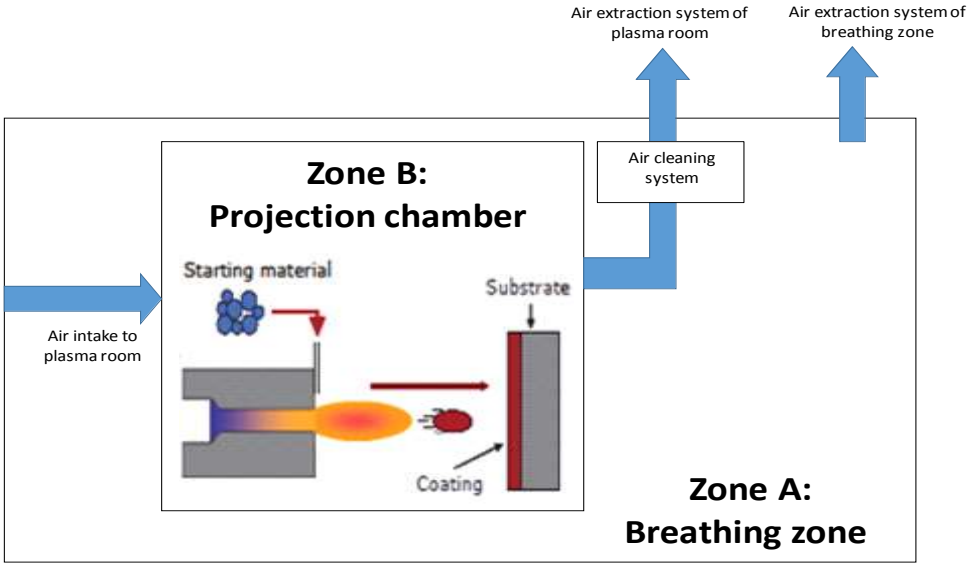

Figure S2. Scheme of plasma projection scenario.

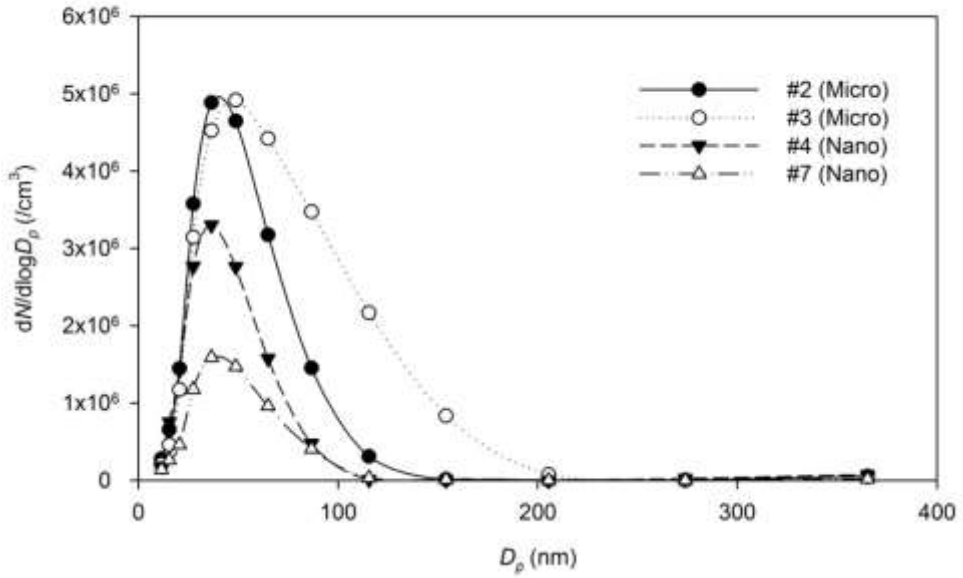

Figure S3. Particle size distribution measured in the plasma chamber during plasma spraying activities: experiment #2 (micro size; mean obtained by 4 replicas for spraying activity), experiment #3 (micro size; 1 replica), experiments #4 (submicron- and nano-sized; 1 replica), and experiment #7 (submicron- and nano-sized; mean obtained by 2 replicas for spraying activity). Particle size distribution for experiments #5 and #6 is not available.